Superconductivity at 33–37 K in $ALn_2Fe_4As_4O_2$ (A = K and Cs; Ln = lanthanides)

Si-Qi Wu,[1] Zhi-Cheng Wang,[1] Chao-Yang He,[1] Zhang-Tu Tang,[1] Yi Liu,[1] and Guang-Han Cao[1,2,3,*]

[1]*Department of Physics, Zhejiang University, Hangzhou 310027, China*

[2]*State Key Laboratory of Silicon Materials, Zhejiang University, Hangzhou 310027, China*

[3]*Collaborative Innovation Centre of Advanced Microstructures, Nanjing 210093, China*

(Received 14 April 2017; published 8 September 2017)

We have synthesized ten iron oxyarsenides, $KLn_2Fe_4As_4O_2$ (Ln = Gd, Tb, Dy, and Ho) and $CsLn_2Fe_4As_4O_2$ (Ln = Nd, Sm, Gd, Tb, Dy, and Ho), with the aid of the lattice-match approach. The resultant compounds possess hole-doped conducting double FeAs layers $[AFe_4As_4]^{2-}$ that are separated by the insulating $[Ln_2O_2]^{2+}$ slabs. Measurements of electrical resistivity and dc magnetic susceptibility demonstrate bulk superconductivity at T_c = 33–37 K. We find that T_c correlates with the axial ratio c/a for all 12442-type superconductors discovered. Also, T_c tends to increase with the lattice mismatch, implying that lattice instability plays a role in the enhancement of superconductivity.

DOI: 10.1103/PhysRevMaterials.1.044804

I. INTRODUCTION

Since the discovery of superconductivity at 26 K in F-doped LaFeAsO [1], many compounds containing FeX (X = As and Se) layers have been found to be superconducting at relatively high temperatures [2,3]. Those materials, known as Fe-based superconductors (FeSCs), have attracted tremendous research interest for their potential applications as well as for the rich underlying physics [3–5]. By utilizing a structural-design strategy, we recently discovered the first double-FeAs-layer FeSC, $KCa_2Fe_4As_4F_2$, with a superconducting transition temperature T_c of 33 K [6]. $KCa_2Fe_4As_4F_2$ crystallizes in a so-called 12442-type structure resulting from an intergrowth between $ThCr_2Si_2$-type (122) and ZrCuSiAs-type (1111) blocks, as shown on the left in Fig. 1. Note that the 122-type KFe_2As_2 is heavily hole doped (0.5 holes per Fe atom), while the 1111-type CaFeAsF is nondoped. Consequently, the 12442-type material by itself is hole doped at a level of 0.25 holes per Fe atom, which makes it superconducting without extrinsic doping. Additionally, there are two distinct As sites in the FeAs layer, similar to the case in 1144-type materials $AeAFe_4As_4$ (Ae = Ca, Sr, and Eu; A = K, Rb, and Cs) [12–15]. The most prominent feature of the 12442 structure lies in its separate double FeAs layers, in analogy with the double CuO_2 layers in cuprate superconductors.

Following the discovery of $KCa_2Fe_4As_4F_2$, we have expanded the 12442-type superconducting family by simple elemental substitutions among alkali metals, which yield two additional fluo-arsenide FeSCs, $ACa_2Fe_4As_4F_2$ with A = Rb and Cs [16]. The T_c values are 30.5 and 28.2 K, respectively. We also succeeded in synthesizing the first 12442-type oxyarsenide, $RbGd_2Fe_4As_4O_2$, whose T_c achieves 35 K [17]. With the substitution of rare-earth elements, four additional oxyarsenides in the Rb-containing series have been found [18]. These studies show that the lattice match between 122 and 1111 blocks is important, as suggested in our earlier proposal [2]. For this reason, the lattice-match paradigm can be employed for the exploration of the remaining 12442-type members. On the right panel of Fig. 1, the lattice parameters a of AFe_2As_2 and LnFeAsO are plotted as the horizontal and vertical coordinates, respectively. In this case, each point with coordinate of (a_{122}, a_{1111}) denotes a 12442-type candidate. The "ideal" lattice match is represented by the lower straight line with $a_{1111} = a_{122}$. In the Rb-containing series (the middle column), the boundary for formation of the 12442 phase is at Ln = Sm, corresponding to the lattice mismatch, parametrized as $2(a_{1111} - a_{122})/(a_{1111} + a_{122})$, of ~2 % [18]. Therefore, we draw the upper-limit line $a_{1111} = 1.02a_{122}$, which could serve as a reference for exploration of the remaining 12442-type oxyarsenides.

In this paper we report ten oxyarsenide FeSCs, $KLn_2Fe_4As_4O_2$ (Ln = Gd, Tb, Dy, and Ho) and $CsLn_2Fe_4As_4O_2$ (Ln = Nd, Sm, Gd, Tb, Dy, and Ho), which are coincidentally located within the shaded area in Fig. 1. Other potential 12442 oxyarsenides outside the shaded area, such as $KSm_2Fe_4As_4O_2$, $RbNd_2Fe_4As_4O_2$, and $CsPr_2Fe_4As_4O_2$, cannot be synthesized at ambient pressure, which further consolidates the crucial role of lattice match for the formation of the intergrowth structure. All these compounds synthesized show bulk superconductivity with T_c = 33–37 K. The maximum T_c of 37 K is observed for $KGd_2Fe_4As_4O_2$. The possible crystal-structure dependence of T_c is discussed in terms of the axial ratio and the lattice mismatch.

II. EXPERIMENTAL METHODS

Samples of $ALn_2Fe_4As_4O_2$ (Ln = Gd, Tb, Dy, and Ho for A = K; Ln = Nd, Sm, Gd, Tb, Dy, and Ho for A = Cs) were synthesized via solid-state reaction processes similar to the previously reported $RbGd_2Fe_4As_4O_2$ [17]. First, source materials of Fe powder (99.998%) and Ln powder (99.9%) were respectively mixed with As granules (99.999%), sealed in evacuated quartz tubes, and heated to 750 °C to prepare FeAs, Fe_2As, and LnAs. An intermediate product of "$A_{1.03}Fe_2As_2$" was then produced by reacting FeAs and A (99.5%) at 600 °C–650 °C for 10 h. After that, stoichiometric mixtures of $A_{1.03}Fe_2As_2$, FeAs, Fe_2As, LnAs, and lanthanide oxides (preheated to 900 °C for 24 h to remove adsorbed water) were ground, pelletized, and finally sintered for 36 h at 940 C°–970 °C in alumina tubes that were sealed in Ta tubes

*ghcao@zju.edu.cn

 ©2017 American Physical Society

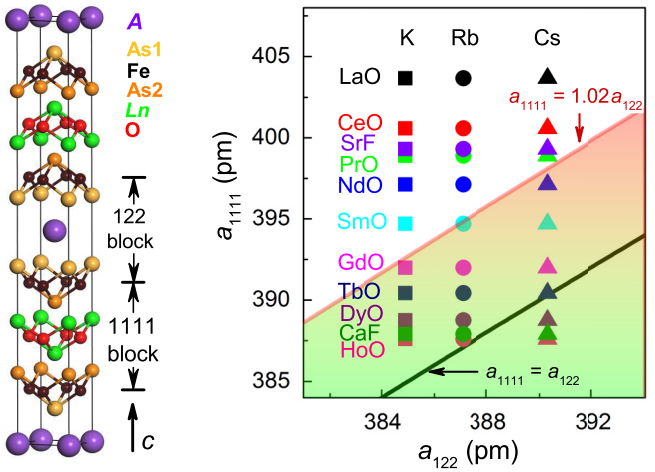

FIG. 1. Lattice match as a crucial factor for the formation of 12442-type $ALn_2Fe_4As_4O_2$ and $ACa_2Fe_4As_4F_2$ (A = K, Rb, and Cs; Ln = lanthanides). On the left is the crystal structure composed of alternating blocks of 122-type AFe_2As_2 and 1111-type $LnFeAsO$ along the c axis. The right panel plots the lattice parameters a [7–11] of the constituent 122 and 1111 iron arsenides as the horizontal and vertical coordinates, respectively. Each point with coordinate of (a_{122}, a_{1111}) in the panel denotes a 12442-type candidate. The lower straight line marks the "ideal" lattice match with $a_{122} = a_{1111}$ and the upper straight line gives the boundary with $a_{1111} = 1.02a_{122}$, beyond which the 12442-type candidates cannot be synthesized at ambient pressure.

jacketed with evacuated quartz ampoules. The final products were found to be stable in air.

We employed a PANalytical x-ray diffractometer with Cu $K\alpha 1$ radiation to conduct the powder x-ray-diffraction experiments at room temperature. The electrical resistivity measurements were carried out via a standard four-probe method on a Physical Property Measurement System (PPMS-9, Quantum Design), with a excitation current of 2 mA. Magnetic properties were measured on a Magnetic Property Measurement System (MPMS-XL5) under a magnetic field of 10 Oe. The samples were cut and polished into rods and the applied field is along the rod direction, which minimizes the demagnetization effect.

III. RESULTS AND DISCUSSION

A. X-ray diffraction

With the consideration of lattice match above, samples with the nominal composition of $ALn_2Fe_4As_4O_2$ (A = K and Cs; Ln = Nd, Sm, Gd, Tb, Dy, Ho, and Er) were prepared using high-temperature solid-state reactions as stated above. Figure 2 shows the powder x-ray-diffraction (XRD) results. In the series of A = K [Fig. 2(a)], the main XRD reflections for Ln = Gd, Tb, Dy, and Ho can be indexed with a body-centered-tetragonal lattice of $a \approx 3.88$ Å and $c \approx 30.6$ Å, consistent with the 12442-type structure. For Ln = Sm, however, no reflections can be identified in the 12442 phase. The final products in the "$KSm_2Fe_4As_4O_2$" sample are actually KFe_2As_2 and SmFeAsO. This is in contrast with the successful synthesis of $RbSm_2Fe_4As_4O_2$ [18], which clearly indicates the thermodynamic instability of $KSm_2Fe_4As_4O_2$ owing to its lattice mismatch (since it is located outside the shaded area in Fig. 1). For Ln = Er, no 12442 phase appears either, although the lattice match seems desirable by extrapolation. Note that

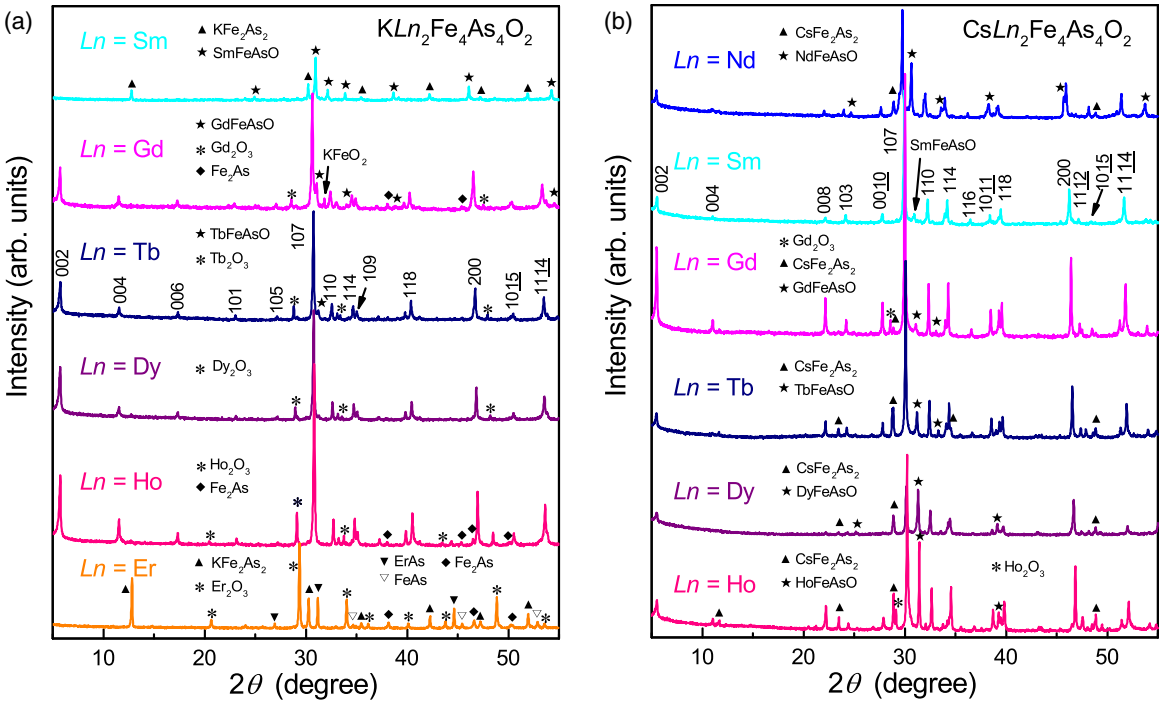

FIG. 2. Powder x-ray-diffraction patterns for (a) $KLn_2Fe_4As_4O_2$ (Ln = Sm, Gd, Tb, Dy, Ho, and Er) and (b) $CsLn_2Fe_4As_4O_2$ (Ln = Nd, Sm, Gd, Tb, Dy, and Ho) at room temperature. The indexed peaks are from the 12442 phase. Other peaks are from impurity phases, which are labeled with different symbols as shown.

TABLE I. Lattice parameters of $KLn_2Fe_4As_4O_2$ (Ln = Gd, Tb, Dy, and Ho) and $CsLn_2Fe_4As_4O_2$ (Ln = Nd, Sm, Gd, Tb, Dy, and Ho) at room temperature.

Compounds	a (Å)	c (Å)
$KGd_2Fe_4As_4O_2$	3.8970(4)	30.670(3)
$KTb_2Fe_4As_4O_2$	3.8862(3)	30.621(3)
$KDy_2Fe_4As_4O_2$	3.8746(6)	30.598(5)
$KHo_2Fe_4As_4O_2$	3.8659(6)	30.597(6)
$CsNd_2Fe_4As_4O_2$	3.9488(14)	32.234(13)
$CsSm_2Fe_4As_4O_2$	3.9256(8)	32.124(8)
$CsGd_2Fe_4As_4O_2$	3.9068(5)	32.051(8)
$CsTb_2Fe_4As_4O_2$	3.8948(5)	31.982(6)
$CsDy_2Fe_4As_4O_2$	3.8877(6)	31.961(9)
$CsHo_2Fe_4As_4O_2$	3.8756(6)	31.949(8)

in this case the final product is a mixture of KFe_2As_2, Er_2O_3, ErAs, FeAs, and Fe_2As. The absence of ErFeAsO in the sample suggests that the failure in obtaining $KEr_2Fe_4As_4O_2$ is mainly due to the instability of ErFeAsO slabs.

The XRD patterns for the A = Cs series are shown in Fig. 2(b). The main phase can be identified as the target 12442-type compounds with Ln = Nd, Sm, Gd, Tb, Dy, and Ho. Similarly, syntheses of "$CsPr_2Fe_4As_4O_2$" and "$CsEr_2Fe_4As_4O_2$" failed because of the lattice mismatch and the instability of ErFeAsO, respectively. Note that the samples with Ln = Nd, Tb, Dy, and Ho contain considerable amount of impurities, although optimization of the synthesis was performed. The impurities are mostly 122 and 1111 phases. This fact suggests that the stability of these compounds is marginal. Namely, the formation energy of the reaction $CsFe_2As_2 + 2LnFeAsO \rightarrow CsLn_2Fe_4As_4O_2$ is nearly zero especially for Ln = Nd and Ho, which ultimately comes from the lattice mismatch.

Remarkably, both $KHo_2Fe_4As_4O_2$ and $CsHo_2Fe_4As_4O_2$ are realized, although HoFeAsO alone cannot be synthesized at ambient pressure. This means that the 12442-type structure may even stabilize the 1111 block. Interestingly, the HoFeAsO phase appears as the secondary phase in the $CsHo_2Fe_4As_4O_2$ sample. We conjecture that it is metastable, which can be formed only at relatively low temperature, possibly as a result of partial decomposition of the 12442 phase.

The lattice parameters can be calculated by using a least-squares fit, as tabulated in Table I. Figures 3(a) and 3(b) plot the resultant lattice parameters of $KLn_2Fe_4As_4O_2$ and $CsLn_2Fe_4As_4O_2$, respectively, as functions of the ionic radii of Ln^{3+} [19]. The unit-cell parameters increase with the ionic radius of Ln^{3+}, as expected. To investigate the lattice-match effect, we also plot the estimated cell parameters $(a_{122} + a_{1111})/2$ and $c_{122} + 2c_{1111}$ for comparison. Indeed, the estimated values basically agree with the experimental results. One would expect $a \approx a_{122} \approx a_{1111} \approx (a_{122} + a_{1111})/2$ for an "ideal" lattice match. However, the best coincidence is seen for $KHo_2Fe_4As_4O_2$ and $CsSm_2Fe_4As_4O_2$, where the lattice match is apparently not perfect. This is due to the interlayer charge transfer, which decreases (increases) the a axis of the 1111 (122) block. A similar phenomenon is observed in the $RbLn_2Fe_4As_4O_2$ series in which the best lattice match is given by Ln = Tb [18]. When a_{1111} is significantly larger than a_{122}, the 122 block is under stretching, such that the resultant a axis is larger than $(a_{122} + a_{1111})/2$. In the case of $a_{1111} \approx a_{122}$, however, the resultant a axis may decrease (owing to the interlayer charge transfer), which leads to the crossings of data in Fig. 3(b). The result indicates that the 122 block is more flexible to accommodate the lattice match. This conclusion is quite reasonable because the 1111 block contains relatively "rigid" Ln_2O_2 layers.

B. Superconductivity

Figure 4 shows the temperature dependence of resistivity, $\rho(T)$ for $KLn_2Fe_4As_4O_2$ (Ln = Gd, Tb, Dy, and Ho) and $CsLn_2Fe_4As_4O_2$ (Ln = Nd, Sm, Gd, Tb, Dy, and Ho). The $\rho(T)$ data indicate metallic conduction with a negative curvature in the high-temperature region. The negative

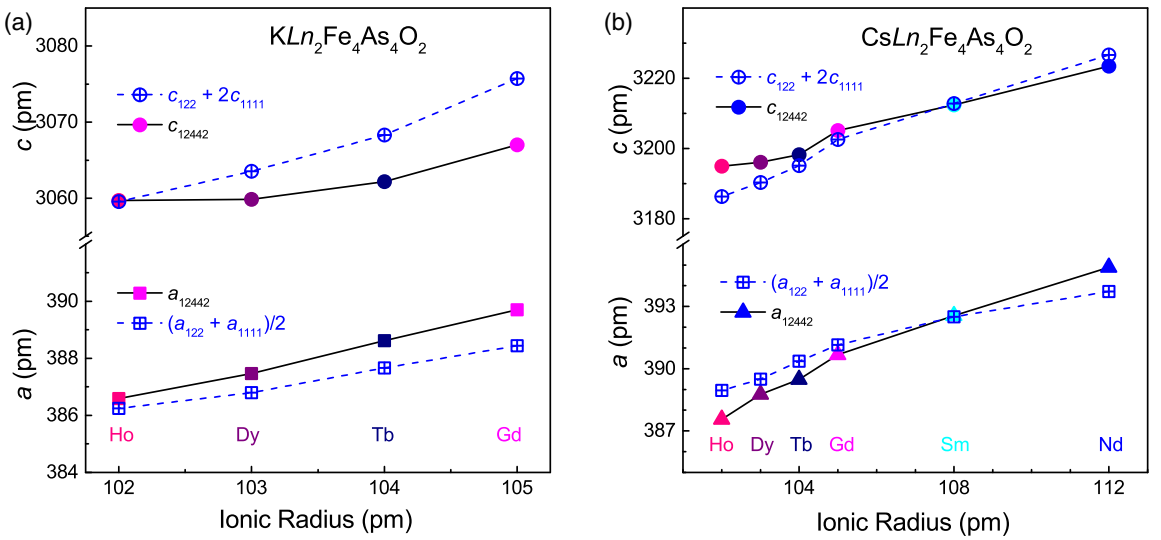

FIG. 3. Lattice parameters of (a) $KLn_2Fe_4As_4O_2$ and (b) $CsLn_2Fe_4As_4O_2$ versus ionic radii of Ln^{3+} [19]. The blue symbols with dashed lines denote the estimated values of the cell parameters from their constituent 122- and 1111-type unit cells [7–9].

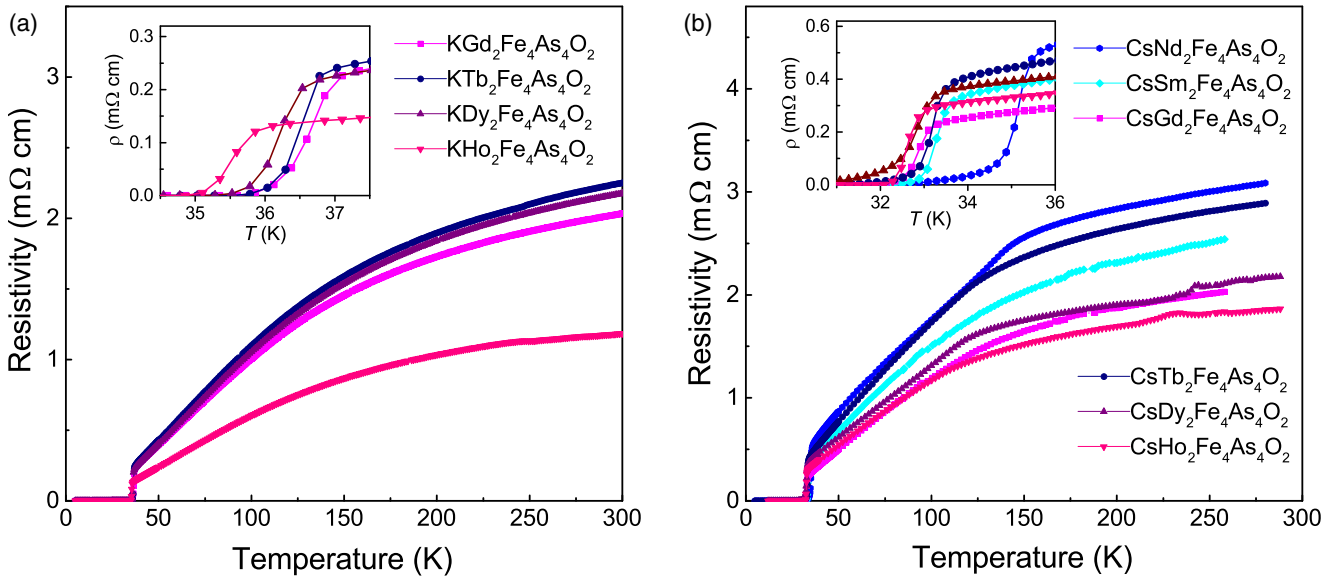

FIG. 4. Temperature dependence of resistivity for the (a) $KLn_2Fe_4As_4O_2$ and (b) $CsLn_2Fe_4As_4O_2$ polycrystalline samples. The insets show close-ups of the superconducting transitions.

curvature differs from the linear behavior expected for dominant electron-phonon scattering. This phenomenon is very often seen in hole-doped FeSCs [6,20,21], which could be related to an incoherent-to-coherent crossover [22]. Note that the kinklike feature at ∼125 K in $CsLn_2Fe_4As_4O_2$ (Ln = Nd, Tb, Dy, and Ho) samples is due to the spin-density wave anomaly of the secondary phase LnFeAsO [9,23], whose existence is detected by the XRD measurement above. The tiny hump at ∼230 K for Ln = Dy and Ho in Fig. 4(b), which is extrinsic to the main phase, possibly comes from a small amount of unknown impurity. One also notes that the normal-state $\rho(T)$ below ∼80 K is essentially linear for the high-purity samples, similar to those observed in other 12442-type FeSCs [6,16–18]. This prominent feature contrasts with the conventional low-temperature T^n ($n \geqslant 2$) behavior due to electron-phonon and/or electron-electron scatterings, suggesting a non-Fermi-liquid behavior.

Superconducting transitions appear at $T_c^{onset} = 36.0$–37.1 K for $KLn_2Fe_4As_4O_2$ and 32.9–35.4 K for $CsLn_2Fe_4As_4O_2$. The transition widths (the difference in temperature at which the resistivity drops to 90% and 10% of the extrapolated normal-state value) are typically about 0.5 K, albeit of a transition "tail" for $CsLn_2Fe_4As_4O_2$ (Ln = Nd and Dy), which contains a relatively large amount of nonsuperconducting secondary phases. Here T_c decreases monotonically with the increase of the atomic number of the lanthanides, akin to the case of Rb-containing series. Note that, in the latter system, the T_c value correlates with the normal-state resistivity [18]. Similar trends can also be seen in the two present systems, even though the samples' quality leads to some interferences.

Superconductivity in $KLn_2Fe_4As_4O_2$ and $CsLn_2Fe_4As_4O_2$ is verified by the dc magnetic measurements. Figure 5 shows the temperature dependence of magnetic susceptibility χ. For clearness, the data in the field-cooling (FC) and zero-field-cooling (ZFC) protocols are plotted separately. First of all, χ_{FC} decreases abruptly at 33–37 K owing to the superconducting Meissner effect. Note that the normal-state susceptibility is mainly contributed from the Curie-Weiss-type paramagnetism of the lanthanide moments. The Meisnner volume fraction, estimated from the magnitude of the χ_{FC} drop, is typically about 10%. Nevertheless, the superconducting shielding fractions, shown in Figs. 5(c) and 5(d), are several times larger. The reduced superconducting signal in the FC mode is very often seen for type-II superconductors (including FeSCs), because of the magnetic-flux pinning when cooling under magnetic fields. For polycrystalline samples, the magnetic shielding fractions better indicate the superconducting volume fraction. The steplike anomaly below T_c for the ZFC data, which also frequently appears for polycrystalline samples of extremely-type-II superconductors, comes from the intergrain weak links. As none of the impurities shows superconductivity above 5 K (only KFe_2As_2 and $CsFe_2As_2$ are superconducting at $T_c = 3.8$ and 2.6 K, respectively [24]), we conclude that the title compounds are responsible for the superconductivity.

C. Discussion

Above we demonstrated that all ten 12442-type compounds show bulk superconductivity at $T_c = 33$–37 K. In fact, the variation in T_c spans nearly 10 K (from 28.2 to 37 K), if the previously discovered 12442-type FeSCs are included. Note that, for a specific 12442-type superconductor, the T_c value hardly changes, regardless of the sample's purity. This means that T_c is intrinsically determined by the material itself, primarily because the material is a line compound (with the stoichiometric composition) that gives rise to a constant hole doping (0.25 holes per Fe atom). We also note that the magnetism of the lanthanide hardly influences the T_c value [18]. Therefore, it is meaningful to examine the crystal-structure dependence of T_c. Our previous investigations [16,18] showed that the T_c trend does not follow the well-known empirical

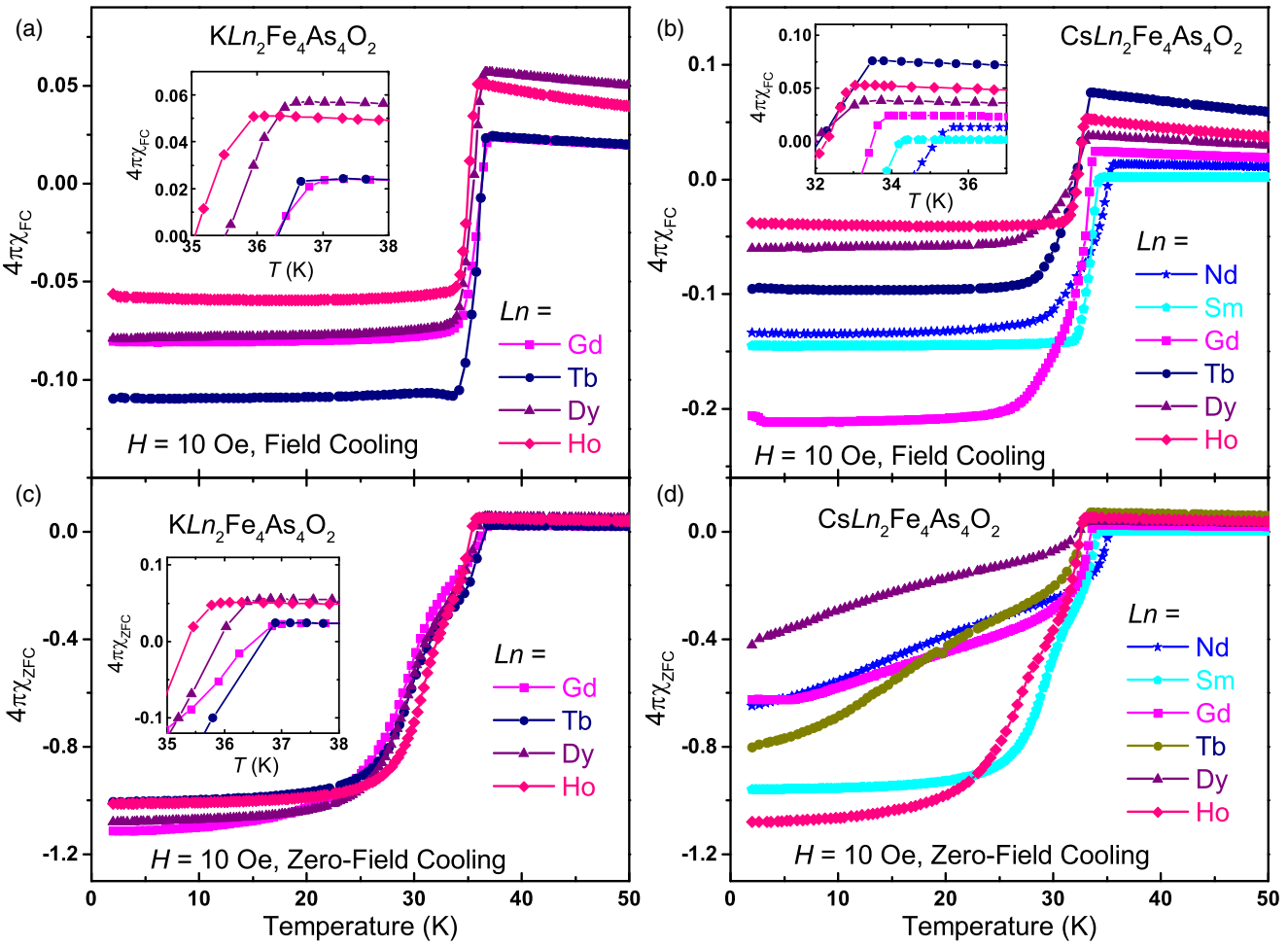

FIG. 5. Temperature dependence of the magnetic susceptibility (in $4\pi\chi$) for (a) and (c) $KLn_2Fe_4As_4O_2$ and (b) and (d) $CsLn_2Fe_4As_4O_2$. Both (a) and (b) field-cooling and (c) and (d) zero-field-cooling data are presented. The insets show close-ups of the superconducting transitions.

rules: The As—Fe—As bond angle [25,26] and the As height from the Fe plane [27] are the two crucial parameters in determining T_c. The possible reason is that the 12442-type FeSCs exceptionally contain double FeAs layers. We found that T_c decreases (increases) with the intrabilayer (interbilayer) spacing [16,18]. In the present K- and Cs-containing series, similar behavior is expected (here we cannot give the structural correlation plot because some samples' purity is not good enough for a reliable structural refinement).

The intrabilayer and interbilayer spacings are defined as the thickness of 122 and 1111 block layers (see Fig. 1) [16,18]. For a certain series, e.g., A = K, while the interbilayer spacing definitely increases with the lanthanide-ion radius, the intrabilayer spacing is actually influenced by the lattice mismatch. As we mentioned above, the 122 block layer is more flexible with respect to the lattice mismatch. If the 122 block is under stretching, intrabilayer spacing is decreased and vice versa. This means that the axial ratio c/a, which is easily accessible, may serve as an effective parameter instead of the intrabilayer spacing. Figure 6(a) plots T_c vs c/a for all 12442-type superconductors. One sees that T_c decreases almost linearly with c/a for each series with A = K, Rb, and Cs. The result suggests that the intrabilayer coupling could enhance the superconductivity.

Now that the change in the intrabilayer spacing results from the lattice mismatch, we also plot T_c vs $2(a_{1111} - a_{122})/(a_{1111} + a_{122})$. As shown in Fig. 6(b), T_c basically increases with the lattice mismatch. The result is actually consistent with the axial-ratio dependence, since a positive lattice mismatch gives rise to a small c/a. Nevertheless, the lattice mismatch also marks the lattice instability. This implies that lattice instability might play a role for the T_c enhancement.

As a matter of fact, the lattice mismatch also generates chemical pressure, the latter of which may substantially affect superconductivity. For each 12442 series with A = K, Rb, and Cs, as shown in Fig. 6(a), T_c tends to decrease with decreasing lattice parameters, which means that positive chemical pressure mildly suppresses the T_c value. In this context, the intrabilayer spacing, lattice mismatch, and chemical pressure are three intertwining factors that control T_c.

So far the highest T_c value is seen in $KGd_2Fe_4As_4O_2$ (37 K) among all eighteen 12442-type FeSCs compounds discovered. It is of great interest whether the T_c value may exceed the record of hole-doped FeSCs (38 K in $Ba_{0.6}K_{0.4}Fe_2As_2$ [20]), since more 12442-type compounds are likely to be discovered. As we previously pointed out, 12442-type compounds with the incorporation of actinides, such as $RbAt_2Fe_4As_4O_2$ (At = Np and Pu), seem to be synthesizable at ambient pressure [18].

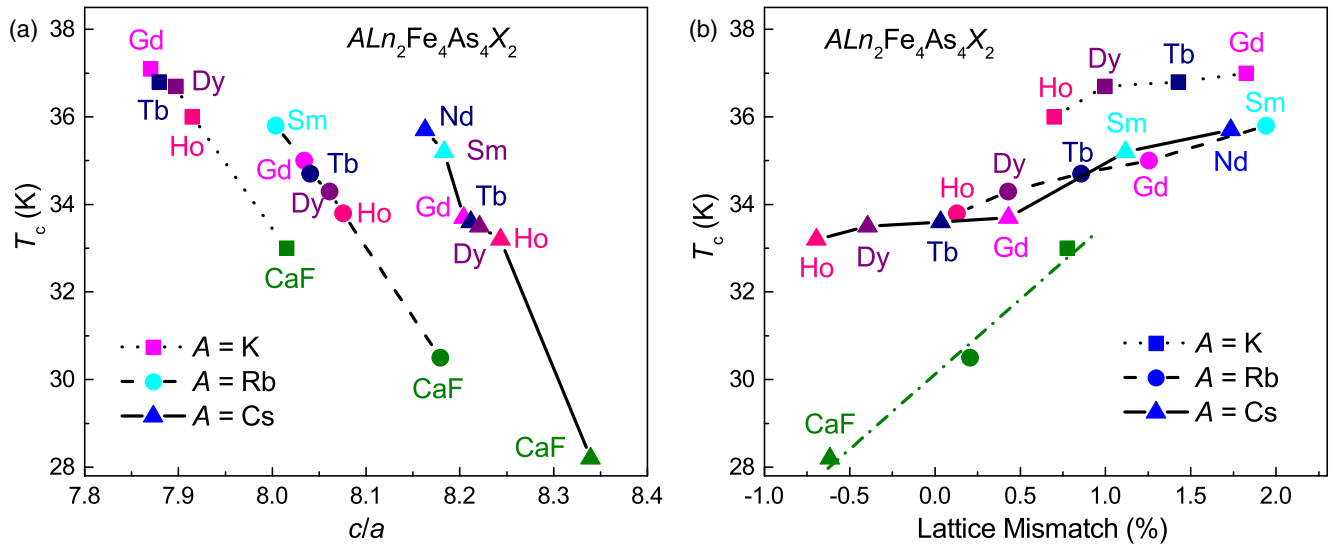

FIG. 6. Influence of (a) c/a and (b) the lattice mismatch $2(a_{1111} - a_{122})/(a_{1111} + a_{122})$ on T_c for all the 12442-type superconductors. Here A, Ln, and X denote alkali metals, lanthanides, and oxygen or fluorine, respectively.

Furthermore, additional metastable 12442-type iron pnictides (say, those outside the shaded area in Fig. 1) could also be realized by high-pressure synthesis.

IV. CONCLUSION

We have reported the syntheses, structural characterizations, and physical-property measurements of ten quinary iron arsenides $ALn_2Fe_4As_4O_2$ (A = K and Cs; Ln = lanthanides). The materials consist of double FeAs layers that are intrinsically hole doped (0.25 holes per Fe atom), which gives rise to the emergence of bulk superconductivity at 33–37 K. The lanthanide-ion magnetism hardly influences the superconductivity. Owing to the unique double-FeAs-layer structure, an additional structural parameter, the bilayer thickness, is found to correlate with the T_c value. At the same time, the lattice mismatch/instability and negative chemical pressure seem to enhance superconductivity congruously. It is of interest for the future to clarify which factor plays the dominant role for superconductivity.

We conclude that the lattice match between the constituent blocks is crucial to stabilize the 12442-type intergrowth structure. Now there are 18 members in the 12442 family, all of which are located in the shaded area in Fig. 1 without exception. This means that the 12442 members containing $5f$ elements Np and Pu are very likely to be synthesized. Furthermore, it is hoped that additional 12442-type FeSCs compounds are to be discovered via a high-pressure synthesis.

ACKNOWLEDGMENTS

This work was supported by the National Key Research and Development Program of China (Grants No. 2016YFA0300202 and No. 2017YFA0303002) and the National Natural Science Foundation of China (Grants No. 11474252 and No. 11190023).

S.-Q.W., Z.-C.W., and C.-Y.H. contributed equally to this work.

[1] Y. Kamihara, T. Watanabe, M. Hirano, and H. Hosono, Iron-based layered superconductor $LaO_{1-x}F_xFeAs$ ($x = 0.05$–0.12) with $T_c = 26$ K, J. Am. Chem. Soc. **130**, 3296 (2008).

[2] H. Jiang, Y.-L. Sun, Z.-A. Xu, and G.-H. Cao, Crystal chemistry and structural design of iron-based superconductors, Chin. Phys. B **22**, 087410 (2013).

[3] H. Hosono and K. Kuroki, Iron-based superconductors: Current status of materials and pairing mechanism, Physica C **514**, 399 (2015).

[4] D. C. Johnston, The puzzle of high temperature superconductivity in layered iron pnictides and chalcogenides, Adv. Phys. **59**, 803 (2010).

[5] X. H. Chen, P. C. Dai, D. L. Feng, T. Xiang, and F. C. Zhang, Iron-based high transition temperature superconductors, Natl. Sci. Rev. **1**, 371 (2014).

[6] Z.-C. Wang, C.-Y. He, S.-Q. Wu, Z.-T. Tang, Y. Liu, A. Ablimit, C.-M. Feng, and G.-H. Cao, Superconductivity in $KCa_2Fe_4As_4F_2$ with separate double Fe_2As_2 layers, J. Am. Chem. Soc. **138**, 7856 (2016).

[7] The lattice parameters of AFe_2As_2 (A = K, Rb, and Cs) are obtained by fitting the powder x-ray-diffraction data of AFe_2As_2 polycrystalline samples. The values are $a = 3.849(1)$ Å and $c = 13.867(2)$ Å for KFe_2As_2, $a = 3.871(1)$ Å and $c = 14.468(2)$ Å for $RbFe_2As_2$; and $a = 3.903(1)$ Å and $c = 15.135(2)$ Å for $CsFe_2As_2$. Those of HoFeAsO, calculated from the secondary-phase reflections in the $CsHo_2Fe_4As_4O_2$ sample, are $a = 3.876(1)$ Å and $c = 8.364(2)$ Å. Note that the lattice parameters of high-pressure-synthesized samples are systematically smaller.

[8] F. Nitsche, A. Jesche, E. Hieckmann, T. Doert, and M. Ruck, Structural trends from a consistent set of single-crystal data of RFeAsO (R = La, Ce, Pr, Nd, Sm, Gd, and Tb), Phys. Rev. B **82**, 134514 (2010).

[9] Y. Luo, X. Lin, Y. Li, Q. Tao, L. Li, Z. Zhu, G. Cao, and Z. Xu, Thorium-doping induced high-T_c superconductivity in $Dy_{1-x}Th_xFeAsO$, Int. J. Mod. Phys. B **26**, 1250207 (2012).

[10] S. Matsuishi, Y. Inoue, T. Nomura, H. Yanagi, M. Hirano, and H. Hosono, Superconductivity induced by co-doping in quaternary fluoroarsenide CaFeAsF, J. Am. Chem. Soc. **130**, 14428 (2008).

[11] X. Y. Zhu, F. Han, P. Cheng, G. Mu, B. Shen, B. Zeng, and H. H. Wen, Parent phase and superconductors in the fluorine derivative family, Physica C **469**, 381 (2009).

[12] A. Iyo, K. Kawashima, T. Kinjo, T. Nishio, S. Ishida, H. Fujihisa, Y. Gotoh, K. Kihou, H. Eisaki, and Y. Yoshida, New-structure-type Fe-based superconductors: $CaAFe_4As_4$ (A = K, Rb, Cs) and $SrAFe_4As_4$ (A = Rb, Cs), J. Am. Chem. Soc. **138**, 3410 (2016).

[13] K. Kawashima, T. Kinjo, T. Nishio, S. Ishida, H. Fujihisa, Y. Gotoh, K. Kihou, H. Eisaki, Y. Yoshida, and A. Iyo, Superconductivity in Fe-based compound $EuAFe_4As_4$ (A = Rb and Cs), J. Phys. Soc. Jpn. **85**, 064710 (2016).

[14] Y. Liu, Y.-B. Liu, Z.-T. Tang, H. Jiang, Z.-C. Wang, A. Ablimit, W.-H. Jiao, Q. Tao, C.-M. Feng, Z.-A. Xu, and G.-H. Cao, Superconductivity and ferromagnetism in hole-doped $RbEuFe_4As_4$, Phys. Rev. B **93**, 214503 (2016).

[15] Y. Liu, Y.-B. Liu, Q. Chen, Z.-T. Tang, W.-H. Jiao, Q. Tao, Z.-A. Xu, and G.-H. Cao, A new ferromagnetic superconductor: $CsEuFe_4As_4$, Sci. Bull. **61**, 1213 (2016).

[16] Z.-C. Wang, C.-Y. He, Z.-T. Tang, S.-Q. Wu, and G.-H. Cao, Crystal structure and superconductivity at about 30 K in $ACa_2Fe_4As_4F_2$ (A = Rb, Cs), Sci. Chin. Mater. **60**, 83 (2017).

[17] Z.-C. Wang, C.-Y. He, S.-Q. Wu, Z.-T. Tang, Y. Liu, A. Ablimit, Q. Tao, C.-M. Feng, Z.-A. Xu, and G.-H. Cao, Superconductivity at 35 K by self doping in $RbGd_2Fe_4As_4O_2$, J. Phys.: Condens. Matter **29**, 11LT01 (2017).

[18] Z.-C. Wang, C.-Y. He, S.-Q. Wu, Z.-T. Tang, Y. Liu, and G.-H. Cao, Synthesis, crystal structure and superconductivity in $RbLn_2Fe_4As_4O_2$ (Ln = Sm, Tb, Dy, and Ho), Chem. Mater. **29**, 1805 (2017).

[19] R. D. Shannon, Revised effective ionic-radii and systematic studies of interatomic distance in halides and chalcogenides, Acta Crystallogr. Sect. A **32**, 751 (1976).

[20] M. Rotter, M. Tegel, and D. Johrendt, Superconductivity at 38 K in the Iron Arsenide $(Ba_{1-x}K_x)Fe_2As_2$, Phys. Rev. Lett. **101**, 107006 (2008).

[21] H.-H. Wen, G. Mu, L. Fang, H. Yang, and X. Zhu, Superconductivity at 25 K in hole-doped $(La_{1-x}Sr_x)OFeAs$, Europhys. Lett. **82**, 17009 (2008).

[22] Y. P. Wu, D. Zhao, A. F. Wang, N. Z. Wang, Z. J. Xiang, X. G. Luo, T. Wu, and X. H. Chen, Emergent Kondo Lattice Behavior in Iron-Based Superconductors AFe_2As_2 (A = K, Rb, Cs), Phys. Rev. Lett. **116**, 147001 (2016).

[23] Y. Luo, Q. Tao, Y. Li, X. Lin, L. Li, G. Cao, Z.-a. Xu, Y. Xue, H. Kaneko, A. V. Savinkov, H. Suzuki, C. Fang, and J. Hu, Evidence of magnetically driven structural phase transition in RFeAsO (R = La, Sm, Gd, and Tb): A low-temperature x-ray diffraction study, Phys. Rev. B **80**, 224511 (2009).

[24] K. Sasmal, B. Lv, B. Lorenz, A. M. Guloy, F. Chen, Y.-Y. Xue, and C.-W. Chu, Superconducting Fe-Based Compounds $(A_{1-x}Sr_x)Fe_2As_2$ with A = K and Cs with Transition Temperatures up to 37 K, Phys. Rev. Lett. **101**, 107007 (2008).

[25] J. Zhao, Q. Huang, C. de la Cruz, S. Li, J. W. Lynn, Y. Chen, M. A. Green, G. F. Chen, G. Li, Z. Li, J. L. Luo, N. L. Wang, and P. Dai, Structural and magnetic phase diagram of $CeFeAsO_{1-x}F_x$ and its relation to high-temperature superconductivity, Nat. Mater. **7**, 953 (2008).

[26] C.-H. Lee, A. Iyo, H. Eisaki, H. Kito, M. T. Fernandez-Diaz, T. Ito, K. Kihou, H. Matsuhata, M. Braden, and K. Yamada, Effect of structural parameters on superconductivity in fluorine-free $LnFeAsO_{1-y}$(Ln = La,Nd), J. Phys. Soc. Jpn. **77**, 083704 (2008).

[27] Y. Mizuguchi, Y. Hara, K. Deguchi, S. Tsuda, T. Yamaguchi, K. Takeda, H. Kotegawa, H. Tou, and Y. Takano, Anion height dependence of T_c for the Fe-based superconductor, Supercond. Sci. Technol. **23**, 054013 (2010).